Impact of annealing treatment on the fatigue behavior of Inconel 625 produced by laser-based powder bed fusion

Noémie Martin, Anis Hor, Etienne Copin, Philippe Lours, Léon Ratsifandrihana

Impact of annealing treatment on the fatigue behavior of Inconel 625 produced by laser-based powder bed fusion

Noémie Martin[1,2] | **Anis Hor**[1] | **Etienne Copin**[1] | **Philippe Lours**[1] | **Léon Ratsifandrihana**[2]

[1]Institut Clément Ader (ICA), Université de Toulouse, CNRS, IMT Mines Albi, INSA, ISAE-SUPAERO, UPS, Toulouse, France

[2]SEGULA Engineering, Immeuble EQUINOX, Colomiers, France

Correspondence
Noémie Martin, Institut Clément Ader (ICA), Université de Toulouse, CNRS, IMT Mines Albi, INSA, ISAE-SUPAERO, UPS, 3 rue Caroline Aigle, 31400 Toulouse, France.
Email: noemie.martin@isae-supaero.fr

Funding information
Segula Technologies

Abstract

Laser-based powder bed fusion (LPBF) is attractive to build complex parts in spite of the low machinability of Inconel 625. The LPBF microstructures and tensile properties are well documented in literature. But fatigue properties and impact of the LPBF intrinsic defects and microstructures on the crack initiation and propagation mechanisms are uncommon. Low and high-cycle fatigue tests at room and service temperature presented in this paper prove that the LPBF defects shorten the crack initiation stage. After annealing heat treatment, the microstructure adapts to the defects, and the fatigue response becomes similar to a free defect material. The fatigue life of as-built Inconel 625 is lower than 50% of its monotonic yield tensile strength (YTS) while the annealed material reaches 100% of its YTS. The propagation rate is slowed by the homogeneous annealed microstructure and improved ductility resulting from removal of dislocation cells and changes in grain morphology.

KEYWORDS

fatigue, heat treatment, Inconel 625, laser-based powder bed fusion

1 | INTRODUCTION

Laser-based powder bed fusion (LPBF) is based on the fusion by laser of metallic powder spread layer wise on a building plate. The high geometrical resolution achievable is attractive to the aerospace and aeronautical fields, where complex parts are produced in limited quantities. Inconel 625 is a solid solution strengthened nickel-based superalloy with outstanding mechanical properties and resistance to corrosion.[1–3] Its conventional machining is difficult and expensive because of excessive tool wear. Yet its excellent weldability makes it a good candidate for LPBF process, keeping the subtractive operations to a minimum. Due to the high solidification and cooling rates during the fabrication process, the microstructure of as-built LPBF Inconel 625 is dendritic, chemically heterogeneous, and out of equilibrium. While these characteristics confer higher elastic and ultimate strengths to the material, it can be anisotropic and has a low ductility.[4] Hence, a heat treatment is necessary to obtain similar monotonic characteristics to the conventional alloy. The fatigue resistance of LPBF Inconel 625 can also be modified by this specific microstructure.[5,6] The present work investigates the mechanical behavior (tensile and fatigue) of as-built and annealed LPBF Inconel 625 at room and at in-service temperature (650°C). The comparison of the two states allows to investigate and explain the impact of the specific LPBF microstructure on the mechanical strength, ductility, and fatigue crack initiation and propagation.

The heat treatment of additively manufactured (AM) Inconel 625 is subject to numerous studies. The optimization criteria vary from chemical homogeneity,[7] maximal mechanical properties[8] to recrystallization.[9]

However, the annealing temperatures usually vary from 1100°C to 1200°C for durations of 1 to 2 h. The conditions depend not only on the treatment's optimization criteria but also on the LPBF material studied. The microstructure and response to treatment change with building parameters, samples orientations, or even among manufacturer or raw powders.[10] For this study, it was previously determined that 3 h at 1150°C followed by a water quench permit to obtain a fully recrystallized and chemically homogenized LPBF Inconel 625, while preserving good mechanical properties.

At first, the monotonic tensile properties are characterized. Plastic flow instabilities are observed during the experimental testing of annealed and as-built LPBF Inconel 625. They are commonly observed in conventional Inconel 625 in literature.[11,12] Some justify these instabilities by the types of grain boundaries,[13,14] but the most consensual explanation is dynamic strain aging (DSA). AM Inconel 625 is also subject to these instabilities, but the observations and conclusions vary from study to study. Some observe the effect at in-service temperatures and link it to both the carbon content and grain boundaries type,[15] some report an absence of effect,[16] and other studies of the LPBF Inconel 625 do not even mention it.[7,17] This paper attempts to summarize the literature's conclusions and proposes an explanation in accordance with the observed results and literature.

The fatigue behavior of LPBF Inconel 625 and the role of the specific defects and microstructure are then investigated. Literature agrees that the fabrication process of Inconel 625 has a strong influence on the fatigue properties. In the early stage of fatigue investigations, the variability of the fatigue properties of materials coming from a single ingot was established.[18] It encouraged the statistical approach. Effects of microstructure, defects, and loading on the fatigue response and limits were investigated on various materials.[19–21] It is now established that for ductile alloys such as nickel-based alloys, the fatigue limit (stress below which no crack can initiate independently to the number of cycles) does not exist.[22] It is hence crucial to understand the causes of variability in fatigue endurance limit at a fixed number of cycles.

Wrought Inconel 625 displays a better high-cycle fatigue endurance than cast and LPBF. It is often imputed to the early crack initiation on specific defects such as porosities.[23] Similar results have been observed by comparing near net-shaped and polished LPBF Inconel 625 fatigue samples.[24] The endurance limit at 2.10^6 cycles is found to be 350 and 400 MPa, respectively, highlighting the importance of surface defects in fatigue life. The limit observed is still inferior to wrought[23,25] Inconel 625 and to the expected standard for Inconel 625, given at 475 MPa for 10^7 cycles.[1] Yet others found a significantly better fatigue resistance for machined LPBF Inconel 625 samples with an endurance at 10^7 cycles of 600 MPa,[26] in spite of systematic crack initiation on lacks of fusion (LoFs). In a defect free material, the initiation takes place on the microstructure weaknesses such as grain boundaries and slip bands.[27] Yet such initiation mechanisms do not necessarily show better endurance limit.[28,29] Hence, the microstructure and grain boundaries present have an impact on initiation too.[30]

Several studies show that fatigue behavior is influenced by the relative size between microstructure and defects.[6] In a defect free material, the fatigue resistance is increased by a fine microstructure.[31] However, in presence of defects, the initiation stage is sensible to the relative size between grains and defects. In the presence of large defects, large grains will be beneficial. It has been shown on steel that the defect sensibility is identical between large grains–large defects and small grains–small defects as long as the ratio is identical.[31] Hence, the variabilities observed in fatigue endurance limits cannot be solely explained by the initiation mechanisms.

The second stage of fatigue rupture is propagation. Propagation rate is known to be complex and impacted by various factors such as loading[19] and microstructure. Dendritic microstructure is known to influence crack propagation in cast Inconel 625.[32] The dendritic cores act as crack propagation units, while the interdendritic zones tend to accumulate dislocations and strengthen. More generally, the dendritic structures can modify the aspect of the failure surface. Tearing of interdendritic zones can be mistaken for fatigue striations, and tearing of cellular dendritic structures can be mistaken for ductile rupture's specific dimples.[33] Hence, the conventional predicting models and relations between the microstructure and fatigue resistance can be modified. While some found that large grain size is detrimental to the fatigue resistance in accordance to Hall–Petch relation,[32,34] others measured a better crack growth resistance in LPBF materials in the case of coarse grains.[29,35]

As discussed, there is no unanimous agreement on the crack initiation and crack propagation mechanisms in LPBF Inconel 625. More investigation is needed to characterize and explain the toughness of the material and the respective importance of initiation and propagation. Moreover, the evolution of the microstructure induced by the heat treatment might change the fatigue resistance. This paper proposes a comparative experimental investigation of as-built and annealed LPBF Inconel 625. Types and size of the defects, as well as the initiation and propagation mechanisms, are identified in order to understand and compare the as-built LPBF Inconel 625 to the annealed, close to the conventional alloy. The

competition between the impact of the microstructure and the impact of defects is investigated, and the benefit of the proposed annealing treatment on fatigue resistance is hence evaluated.

This paper is organized in five sections. Section 2 details the LPBF powder's characteristics and the fabrication parameters, as well as the various experimental observations and testing techniques used in the study. In Section 3, as-built and heat-treated LPBF Inconel 625 are compared in terms of microstructures (grains morphology and texture), mechanical properties, and fatigue resistance at room and service temperature. Sections 4 and 5 are dedicated to the discussion of the experimental results in light of the literature and highlight the originality of the results and analysis conducted.

2 | MATERIALS AND METHOD

2.1 | Samples fabrication and annealing treatment

Inconel 625 LPBF samples were fabricated on a SLM Solution 125HL machine with $125 \times 125\ mm^2$ steel building plates. The standard fabrication parameters used are given in Table 1a. The powder used was supplied by SLM Solution. The chemical composition and powder size distribution deciles provided by the supplier are given in Table 1b. It is in accordance with the standard UNS N06625 defining the super alloy IN625.

The built samples were cut from the building plate by electric discharge machining and heat treated in a preheated furnace at 1150°C, in still air. After a hold of 3 h, they were water quenched. Temperature measurements using S-type thermocouple showed that the target temperatures were respected at ±1°C.

Samples used for microstructural characterization are $10 \times 10 \times 10\ mm^3$ cubes. For the room temperature tensile and fatigue test, the specimen was near net shaped directly by LPBF process (Figure 1A). For the in-service temperature tensile and fatigue test, the specimen was machined from 20-mm-diameter cylinders (Figure 1B). Finally, all fatigue samples were polished on an in house-made semiauto machine, with a principle close to belt-polishing with a contact force kept to a minimum. The finishing stage consisted in 10-μm-sized abrasive diamond suspensions.

2.2 | Microstructural observations

The $10 \times 10 \times 10\ mm^3$ cubes were used for the microstructure observations after polishing and etching with Regal solution (30% HNO_3 70% HCl) steps. Microstructure was observed at different scales by optical and scanning electron microscopes. The electron backscattered diffraction (EBSD) analyses were carried out using a JSM-7100 TTLS LV equipped with an HKL EBSD system. The dimensions of the EBSD maps was 2.1 mm × 1.6 mm. The EBSD measurements were post treated using MTEX Libraries.[36] Misorientations above angles of 10° and delineating a minimal grain area of 10 pixels (20 μm^2, 2.5-μm equivalent diameter) are considered as grain boundary. The twin boundaries are determined as a misorientation of 60°+/5° twisted about the (111) plane. The misorientation between 3° and 10° are calculated as low-angle grain boundaries. The total length of each boundary type is calculated. The proportion of twinning monitors, the evolution of the recrystallization phenomenon, and the proportion of subgrain boundaries are directly related to intragranular misorientations and thus dislocation densities.[37]

TABLE 1 LPBF fabrication conditions (a) SLM solution Inconel 625 standard fabrication parameters and (b) granulometry and chemical composition of the SLM solution Inconel 625 powder

a.

Energetic parameters		**Lasing strategy parameters**	
Laser power	275 W	Hatch distance	0.12 mm
Laser speed	760 mm/s	Hatch stripe length	10 mm
Layer thickness	0.05 mm	Rotation layer to layer	67°
Building plate temperature	200°C		

b.

Powder size (μm)	**Chemical composition (wt.%)**						
$D_{10} = 21$	Ni	Cr	Mo	Nb + Ta	Fe	Co	Si
$D_{50} = 34$	61.14	21.41	8.99	3.69	4.13	0.16	0.09
$D_{90} = 54$	Mn	Ti	Al	C	S	P	
	0.03	0.05	0.04	0.03	0.001	0.005	

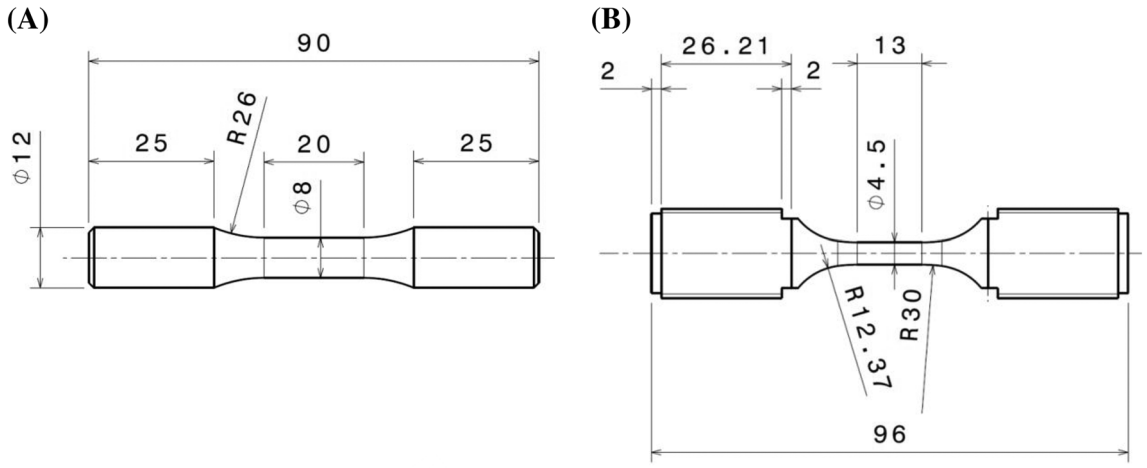

FIGURE 1 Tensile and fatigue specimens for (A) room and (B) 650°C in-service temperatures

Finally, the density of the material was measured by X-ray tomography. The tension and intensity used were 130 kV and 61 μA, to the maximum capacity of the equipment. The work distance was minimized to obtain a voxel size of 5 μm, highest resolution achievable with this equipment on metallic material, and for the volume analyzed (cylinders of 4-mm diameter, 5-mm height).

2.3 | Mechanical characterization

Several mechanical tests have been carried out:

- The room temperature tensile tests were performed up to failure on an INSTRON-5902 machine at a strain rate of $1.25 \times 10^{-3}\ s^{-1}$ using strain control determined by video extensometer.
- The room temperature high-cycle fatigue tests were carried out on a uniaxial MTS 810 100-kN machine using load control. The conditions were tension–tension sinusoidal signals with a load ratio of $R = 0.1$ and a frequency of 15 Hz. Each test was carried out until failure, except if the conventional fatigue life of 2.10^6 cycles was exceeded. In this case, the load level was considered as the high-cycle fatigue endurance.
- The tensile and fatigue tests at the in-service temperature of 650°C were performed on a uniaxial Schenk 250 kN equipped with a radiative furnace AET 1000°C. The homogeneity of the temperature was verified with thermocouples on a test sample: three measurements on the vertical and three around the section. The elongation of the sample is measured by a Schenk ceramic extensometer with a gauge length of 10 mm and maximal measurable elongation of 10%. The elongation at failure is approximated from the machine displacement and sample initial length of interest. The in-service temperature fatigue tests are strain-controlled triangular signals with a strain ratio of $R = -1$ and a strain rate of $10^{-3}\ s^{-1}$.

For each type of sample, three tensile tests are performed. The yield tensile strength (YTS) is determined as the stress at 0.2% elongation, using the Young modulus calculated from the strain–stress curves. The ultimate tensile strength (UTS) given is the maximal load divided by the initial section. These characteristics and the maximal elongation (A, %) are given as the average of the three tests conducted and an envelope containing the minimum and maximum values.

3 | EXPERIMENTAL RESULTS: COMPARISON BETWEEN AS-BUILT AND HEAT-TREATED INCONEL 625

3.1 | As-built and treated microstructures

Inconel 625 obtained by LPBF process displays melt pools of about 0.1-mm width and depth visible on Figure 2A by scanning electron microscopy (SEM). These observations show that the microstructure is dendritic with columnar and cellular cells of 1-μm width visible by chemical contrast. The high solidification rates involved in LPBF process induce the microsegregation of niobium and molybdenum. These heavy elements remain in the interdendritic zones, leading to a heterogeneous solidified material as illustrated by the energy-dispersive X-ray analysis (EDX) measurements on Figure 3. The crystallographic structure of the as-built Inconel 625 presents elongated grains oriented along the shape of the melt pool, as shown on the grain orientation map

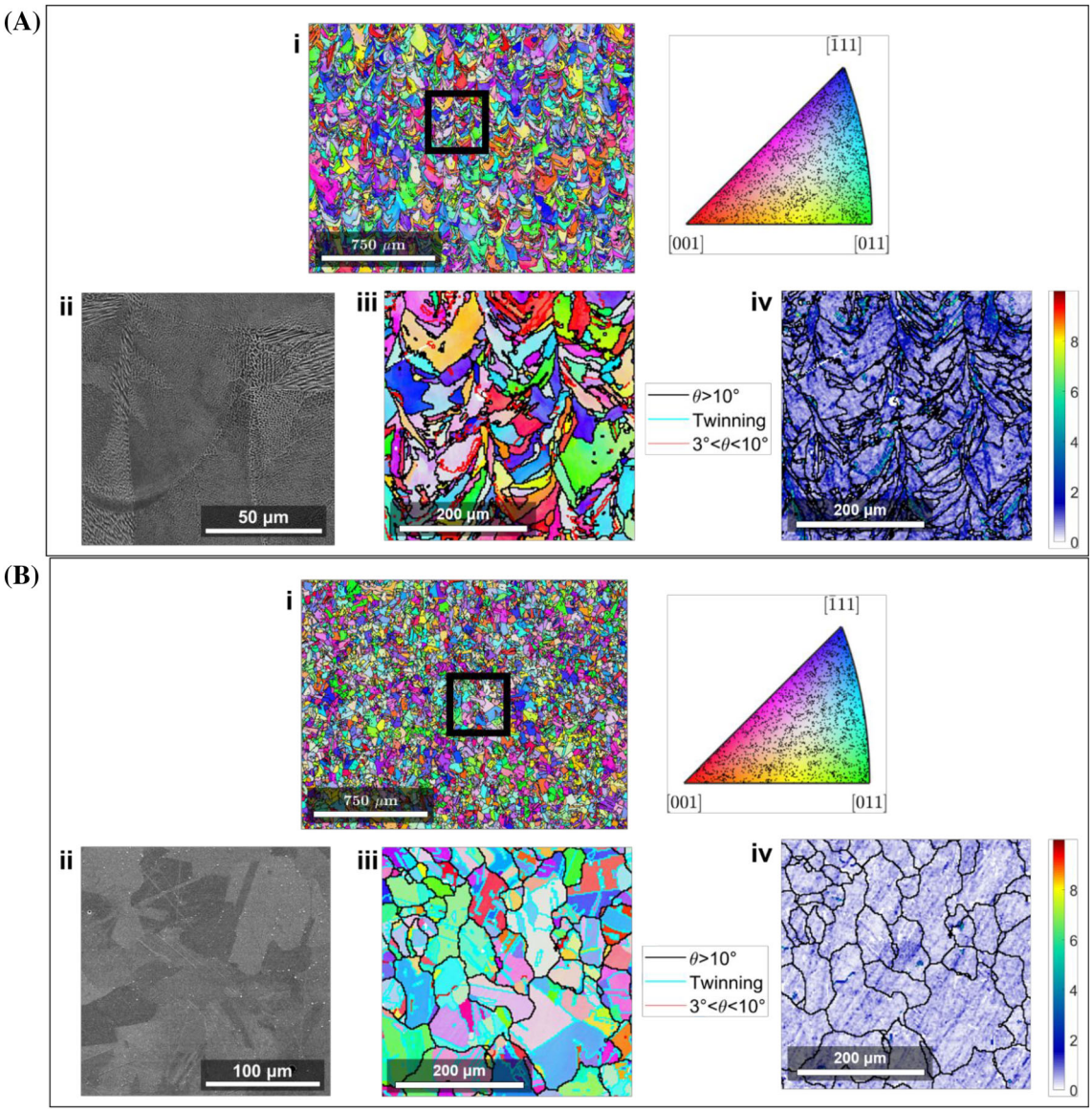

FIGURE 2 (A) As-built and (B) annealed LPBF Inconel 625: (i) *Z*-axis IPF map and key, details: (ii) SEM image, (iii) types of grain boundaries, and (iv) kernel average misorientation [Colour figure can be viewed at wileyonlinelibrary.com]

(inverse pole figure [IPF]) from EBSD analysis displayed in Figure 2A. This microstructure depends on the building strategy and is consistent with literature.[38,39] Using EBSD analysis, the mean of the grain equivalent diameter is 11 μm with a standard deviation of 7 μm.

An annealing treatment of 3 h at 1150°C followed by a water quench allows dissolving the dendritic structures. The resulting homogeneous microstructure is shown on Figure 2B.ii, where occasional carbides are visible on the grain boundaries. In terms of crystallographic structure, the heat-treated Inconel 625 has equiaxial grains with frequent twinning boundaries (Figure 2B.iii). The recrystallization and grain growth during the heat treatment lead to an average equivalent diameter of 24 μm with a standard deviation of 18 μm.

In addition to the high solidification rate, the local and significant temperature gradients during the LPBF process induce residual stresses in the part and at the crystal scale in the form of dislocations. The dendrites favor the entanglement of the dislocations and hinder their movement. Studies on 316L steel and Inconel 718 showed that the dislocations cells organized around the dendrites are dissolved during heat treatment.[40,41] They used transmission electron microscopy (TEM) to investigate the dislocations behavior, but the dislocation density evolution is detectable by EBSD measures via the intergranular misorientation as the kernel average misorientation (KAM) or low-angle grain boundaries.[7,37] In the as-built material of this study, low-angle grain boundaries represent 13% of the total boundaries' length. After

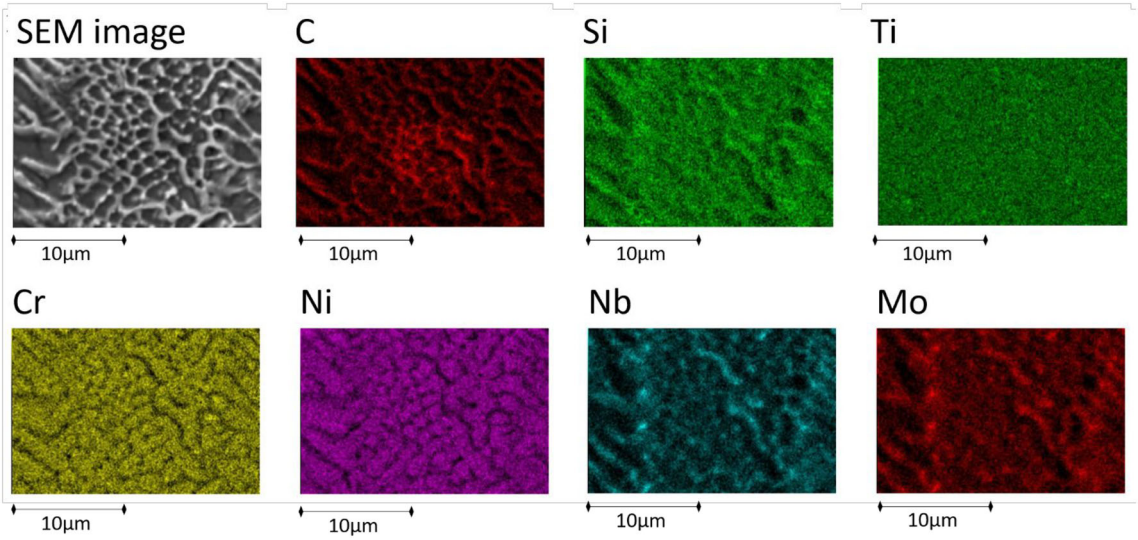

FIGURE 3 EDX mapping of as-built LPBF Inconel [Colour figure can be viewed at wileyonlinelibrary.com]

TABLE 2 Properties obtained from tensile tests on LPBF Inconel 625 at room and service temperatures along results on wrought Inconel 625 from the ASM Handbook[1]

	Room temperature			In-service temperature of 650°C		
	As built	Annealed	Wrought[1]	As built	Annealed	Wrought[1]
YTS (MPa)	667 ± 3	363 ± 4	490	521 ± 13	310 ± 1	420
UTS (MPa)	939 ± 1	853 ± 5	855	721 ± 1	751 ± 4	710
A (%)	39 ± 2	62 ± 2	50	52 ± 2[a]	83 ± 5[a]	35

[a]Calculated from the total displacement.

the treatment, it represents less than 1%. The dislocations are annihilated during the treatment, consistent with the tendency demonstrated by TEM measures in literature. A qualitative comparison of the KAM of as-built (Figure 2A.iv) and heat treated (Figure 2B.iv) confirm that internal granular misorientation is annealed after 3 h at 1150°C.

Finally, the density of the as-built material is determined by X-ray tomography. The principal defects encountered in LPBF Inconel 625 are spherical voids resulting from entrapped gas and LoFs. The analyzed volumes were cylinders with a diameter of 4 mm and a height of 10 mm machined by EDM from the core of the samples. The voids detected with tomography were evenly distributed and spherical. The total volume fraction was 0.02%. The average equivalent diameter of defect is 13 µm with a standard deviation of 16 µm (maximal size of detected defect is 32 µm). It must be emphasized that the voxel size limits the type of defects detected. The interlayer LoFs can be thin and hence not visible nor accounted for by X-ray tomography. Moreover, LPBF induces specific defects at the extreme surface of samples (200 µm).[29] The cylindrical tomography samples being taken from the core of the samples, this zone was not characterized. Yet the polishing of the fatigue samples is believed to remove the surface.

3.2 | Tensile properties of both microstructures

Table 2 sums up the tensile properties obtained at room temperature and at 650°C. At both temperatures, the as-built LPBF Inconel 625 displays higher yield and ultimate stress than the annealed material but lower maximal elongation. At room temperature, the total elongation for the as-built material is 39%, but after an annealing treatment, it is higher than 60%, which is very satisfactory compared to standards for wrought Inconel 625.[1] The in-service temperature softens the resistance of both as-built and annealed LPBF Inconel 625 and increases significantly their ductility (52% for as built, 83% for annealed condition).

Figure 4 shows the tensile curves obtained for one as-built sample and one annealed sample at room and in-service temperature. For each batch, all the tensile curves are very similar due to a good repeatability in the tests. LPBF Inconel 625 was subject to serrations at room and

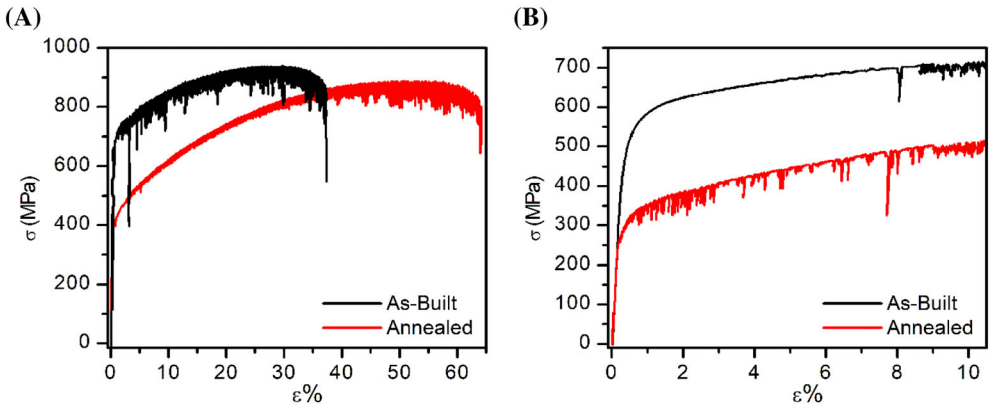

FIGURE 4 (A) Room temperature and (B) 650°C service temperature tensile tests of LPBF Inconel 625 [Colour figure can be viewed at wileyonlinelibrary.com]

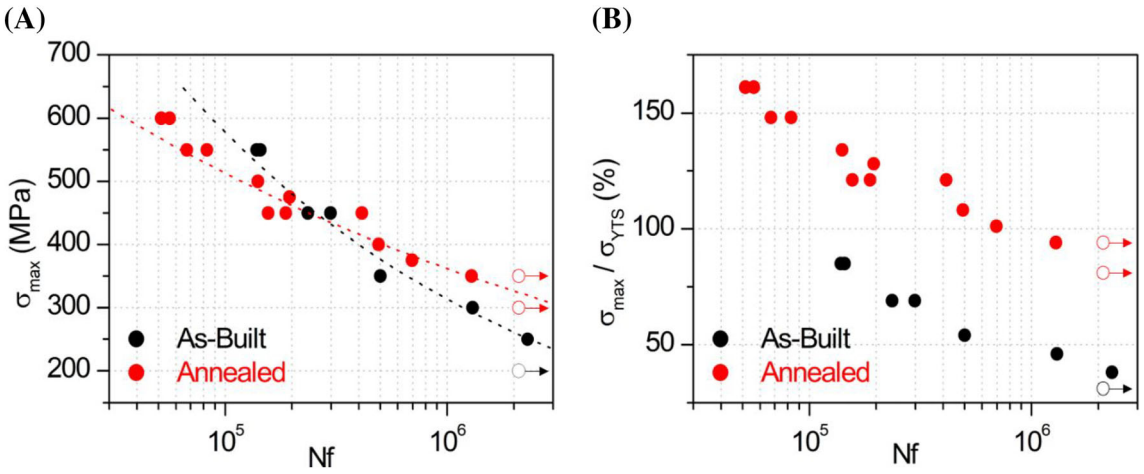

FIGURE 5 (A) Wöhler curve and (B) Wöhler curve with maximal stress expressed as YTS percentage for as-built and annealed LPBF Inconel 625. Room temperature high-cycle fatigue tests, $R = 0.1$ [Colour figure can be viewed at wileyonlinelibrary.com]

in-service temperatures, Figure 4A,B, respectively. The instabilities in the plastic flow are known as the Portevin–Le Châtelier (PLC) effect. They are common in nickel-based alloys but are usually observed at high temperatures.[42] The PLC effect and the serrations are highly sensitive to the testing conditions (strain rate, stress or strain or displacement control ...). At room temperature, the amplitudes and frequency are more regular throughout the tensile tests. At 650°C, large punctual serrations occur randomly during the plastic deformation. Also, the plastic flow of the as-built material is stable before 8% deformation, while the perturbations appear directly on the heat-treated Inconel 625.

3.3 | Room temperature stress-controlled fatigue behavior

Stress-controlled fatigue tests have been conducted to identify the high-cycle fatigue behavior of LPBF Inconel 625. The Wöhler curves obtained are given on Figure 5A, along with the exponential law defined by Stromeyer[18] in 1914 and commonly used in literature[43,44] which fits the experimental data in this high-cycle fatigue tests with imposed fatigue life. The difference in steepness of the approximation highlights that annealed LPBF Inconel 625 is slightly more sensitive to the load level than the as-built material. Yet the as-built LPBF Inconel 625 has a fatigue endurance lower to 250 MPa while after the annealing treatment, it can withstand around 350 MPa for 2.10^6 cycles. The limit of 250 MPa for the as-built material is significantly lower than its YTS of 667 MPa, while the limit of 350 MPa for the annealed material is around the same order of the corresponding YTS value. Figure 5B illustrates this difference between the as-built and the annealed microstructures by plotting the Wöhler curve with the percentage of YTS instead of the maximal stress applied.

The cyclic responses of the as-built and annealed microstructures at the same stress level are illustrated on Figure 6. In the as-built case, the behavior is elastic during the first cycles as the maximal load level is lower

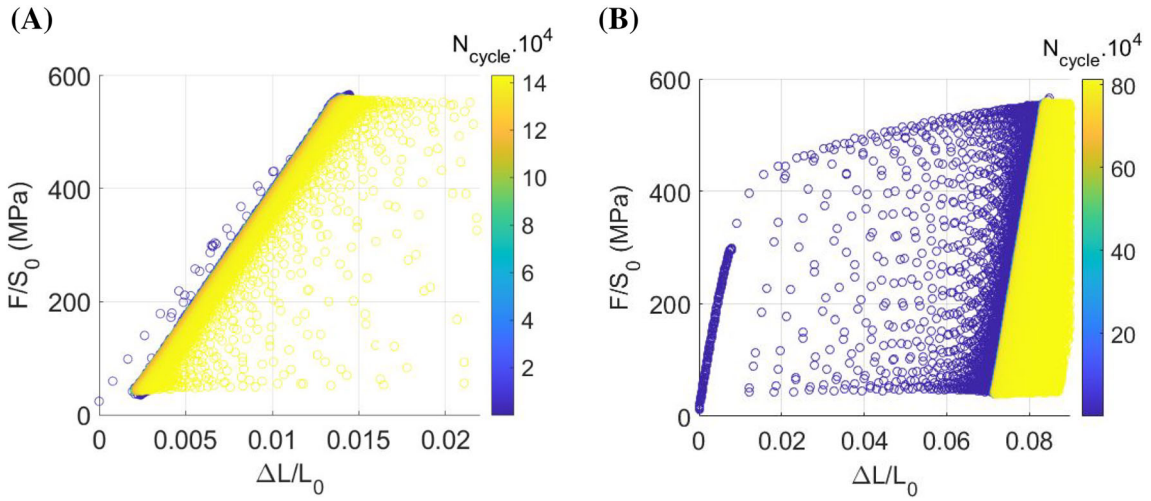

FIGURE 6 Cyclic behavior of (A) the as-built and (B) the annealed microstructures at the same stress level: between 55 and 550 MPa. Room temperature high-cycle fatigue tests, $R = 0.1$ [Colour figure can be viewed at wileyonlinelibrary.com]

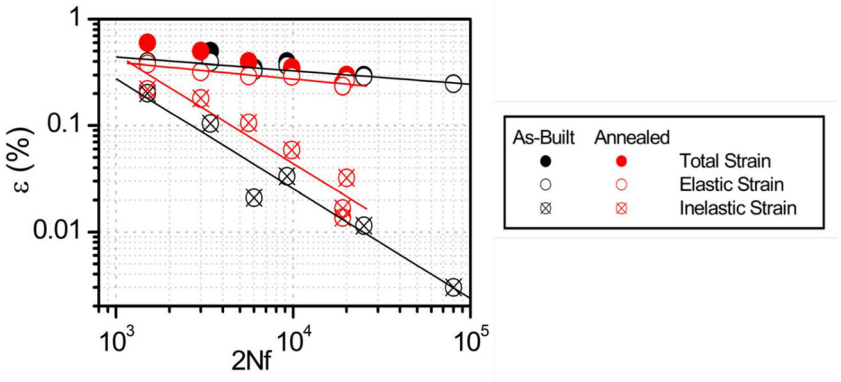

FIGURE 7 Fatigue life diagrams for as-built and annealed LPBF Inconel 625 along with the Basquin and Manson–Coffin approximations. $R = -1$, 650°C low-cycle fatigue tests [Colour figure can be viewed at wileyonlinelibrary.com]

than the YTS. However, an elastic shakedown is observed after a few cycles in the case of annealed LPBF Inconel 625.

3.4 | In-service temperature strain-controlled fatigue behavior

The low-cycle fatigue behavior of LPBF Inconel 625 at 650°C was investigated using strain-controlled fatigue tests. The maximal strains investigated range between 0.25% and 0.6%. The obtained strain-fatigue diagram is given on Figure 7. The total strain is decomposed into the elastic strain, leading to Basquin's law, and plastic strain, leading to Manson–Coffin's law. For a given total strain solicitation, as-built and annealed LPBF Inconel 625 have similar fatigue life. The plain dots on the diagram Figure 7 coincide. Yet, for a given plastic strain (crossed dots on Figure 7), the annealed LPBF Inconel 625 roughly doubles its fatigue life compared to the as-built material.

The strain–stress hysteresis loops given in Figure 8 describe the response of the as-built and annealed LPBF Inconel 625 at the strain rate of ±0.3% and ±0.6%. The behavior observed for the as-built microstructure is stable and quasielastic at 0.3% and elastic–plastic at 0.6%. A slight cyclic hardening behavior is observed for the high strain (0.6%). In the case of the annealed material, the response to 0.3% strain evolves from an elastic–plastic behavior to a quasielastic behavior for the last cycles before failure. For high strain (0.6%), the shape of the loop evolves too, with a clear cyclic hardening phenomenon.

The cyclic hardening/softening can be also illustrated by plotting the stress amplitude as a function of the cycle number (Figure 9). Both the materials are subject to cyclic hardening, but the extent and rate of the phenomenon is higher in annealed LPBF Inconel 625. The stress amplitude difference between the first cycles and the last cycles has reached +88% at 0.6% and +55% at 0.3% (Figure 9B) against +25% and +8% for the as-built microstructure (Figure 9A).

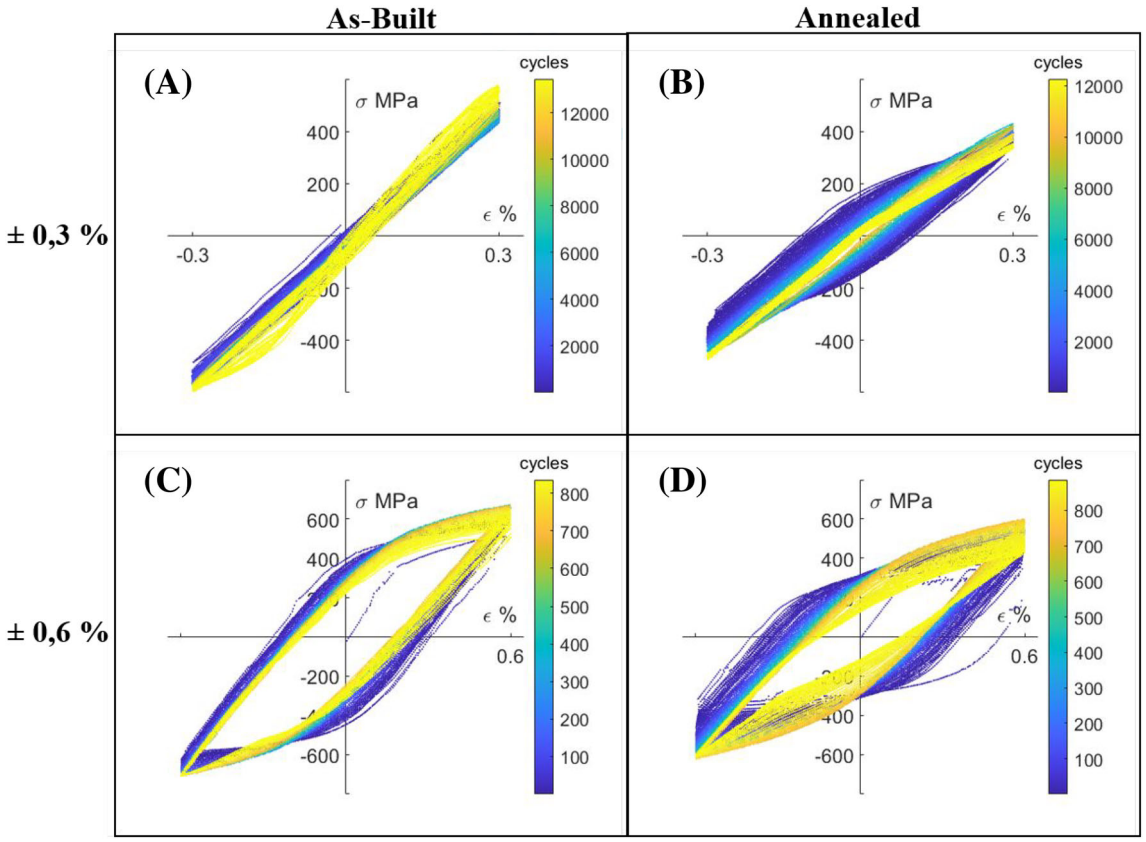

FIGURE 8 Hysteresis loops for (A,B) as-built and (C,D) annealed LPBF Inconel 625 solicited at (A,C) ±0.3% and (B,D) ±0.6% during $R = -1$, 650°C low-cycle fatigue tests [Colour figure can be viewed at wileyonlinelibrary.com]

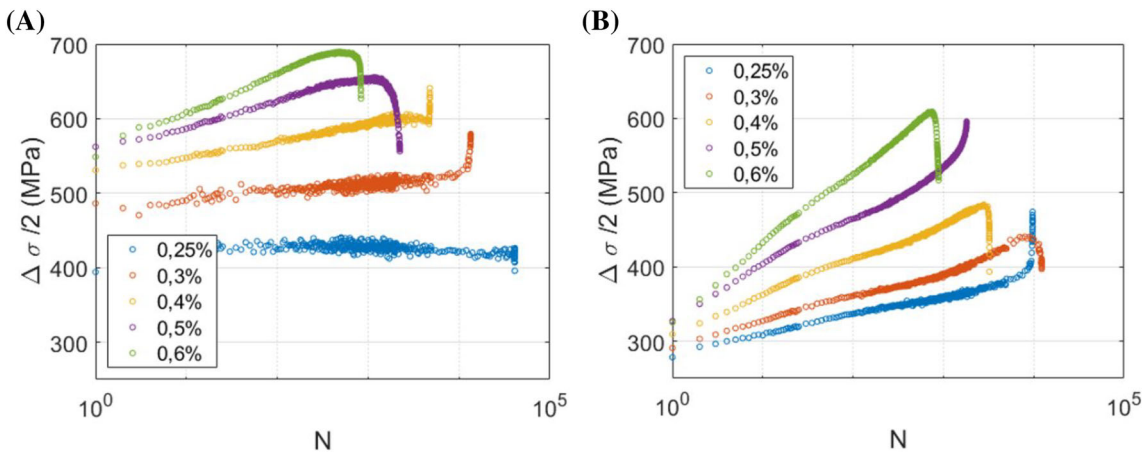

FIGURE 9 Cyclic hardening curves for (A) as-built and (B) annealed LPBF Inconel 625 during $R = -1$, 650°C low-cycle fatigue tests [Colour figure can be viewed at wileyonlinelibrary.com]

4 | ANALYSIS AND DISCUSSIONS

4.1 | Origin of PLC effect in LPBF Inconel 625

The instabilities in the plastic behavior observed during the tensile tests (Figure 4) are known as the PLC effect and are widely attributed to DSA. The dynamic interactions between mobile dislocations and solute atoms can alter the macroscopic mechanical properties. They are sensitive to temperature and strain rates. Two mechanisms causing those interactions were identified in literature.[45] The first mechanism hindering the dislocation mobility is known as "line strengthening." A dislocation

distorts the crystal and induces a zone with tensile stress below its edge. The solute atoms tend to diffuse to this zone and can be dragged by the dislocation when it moves. The second mechanisms are based on the interaction between mobile and static dislocations. A rapid "pipe diffusion" of the solute occurs when they interact, leading to immediate line strengthening. Simultaneously, a flock of solute atoms is formed around the intersection of the dislocations, causing dislocation hindering known as the "intersection strengthening."

In Ni-based alloys, DSA is induced by different elements according to the temperature.[42] At room temperature, some studies showed that the PLC effect is caused by the interstitial diffusion of carbon atoms.[9,16] Carbon is known to be responsible for DSA in bielement Ni–C alloy. At high temperatures, the element widely identified to be responsible for the DSA is molybdenum, based on the calculated activation energy[46,47] and experimental internal friction tests with spectroscopy.[42] The differences observed between the tensile tests carried at room and in-service temperature (Figure 4) seem to confirm that the phenomenon happening are different.

At room temperature, as-built and heat-treated LPBF Inconel 625 have similar plastic flow behaviors. The serrations in the as-built microstructure have random frequency and greater amplitudes than the annealed microstructure. In both microstructures, the instabilities appear right at the beginning of the plasticity. At 650°C, the as-built microstructure displays a critical deformation $\varepsilon_c \in [3\%;8\%]$ until which the stress–strain curve is stable. The serrations begin only after. In the annealed samples, the serrations appear immediately after the yield stress. The amplitudes and frequencies are comparable.

Based on the literature discussed above, the chemical inhomogeneity of the LPBF Inconel 625 illustrated by EDX measures on Figure 3 can be responsible. At room temperature, no clear difference in as-built and treated Inconel 625 is observed. If, as suggested by literature,[9,11] carbon interstitial diffusion and interaction with the solutes is responsible, it would mean the microsegregation of the element observed in Figure 3 does not impact the phenomena. Nakada and Keh[11] investigated the behavior of Ni–C alloy and showed that at room temperature and for a strain rate of 10^{-3} s^{-1}, a carbon concentration of 0.075% and below does not affect the serrations or the critical strain which is inferior to 0.1%. In this study, the Inconel 625 used contains less than 0.03% carbon. This could explain the similar behavior between as-built and treated materials in this case. Further quantitative investigation such as tests on Inconel 625 with various carbon concentrations would be needed to confirm this hypothesis.

At 650°C, molybdenum interactions with the dislocations is believed to be responsible for the PLC effect,[42,46,47] unlike the carbon that diffuses interstitially. In the as-built material, molybdenum is subject to microsegregation illustrated in Figure 3. Moreover, the dislocations are known to be organized in cells and entangled. This heterogeneity and dislocation entanglement are believed to prevent the mechanisms of line and intersection strengthening. The first part of the plastic flow rearranges the dislocations initially organized as cells around the dendritic structures before the dislocation–molybdenum interactions can occur. The annealed LPBF Inconel 625 is a quasihomogeneous solid solution of Nb and Mo in a Ni matrix. Line and intersection strengthening can occur from the beginning with the solutes dissolved in the matrix. The critical strain observed in the as-built material could hence be justified. Similarly, further experiment with various molybdenum repartition and dislocation densities is required to validate this hypothesis based on literature review.

4.2 | Effect of heat treatment on high-cycle fatigue strength

The high-cycle fatigue strength of the as-built LPBF Inconel 625 is below the resistance of the annealed material. Yet the as-built YTS is higher than the annealed YTS (667 MPa against 363 MPa; Table 2). The fatigue resistance is about 50% of the YTS for the as-built microstructure, while the order of magnitude after the annealing treatment is 100% of the YTS, as illustrated by Figure 5B. The room temperature high-cycle fatigue behavior of annealed LPBF Inconel 625 is close to a theoretical defect free material, where failure happens only for solicitations inducing plastic deformation.[26] Moreover, the samples observed revealed that for a similar number of cycles, the propagation area in the as-built samples is greater than the annealed as illustrated by Figure 10. This remains true for high and low stress levels. The overall propagation rate is slowed down by the microstructure after the annealing treatment.

Observations of the fractured surfaces revealed that as-built and annealed samples presented multicrack fractures and initiated from defects on different layers of fabrication. Initiation sites were LoFs open to the surface or in the subsurface of the sample. LoFs are smooth surfaces, with occasional grains of powder that were not completely melted, as indicated in red on Figure 11. The sizes of the defects where a crack initiation occurred were measured from their surfaces, as an equivalent diameter (same technique as for the grain size). The mean equivalent diameter of all defects responsible for an initiation

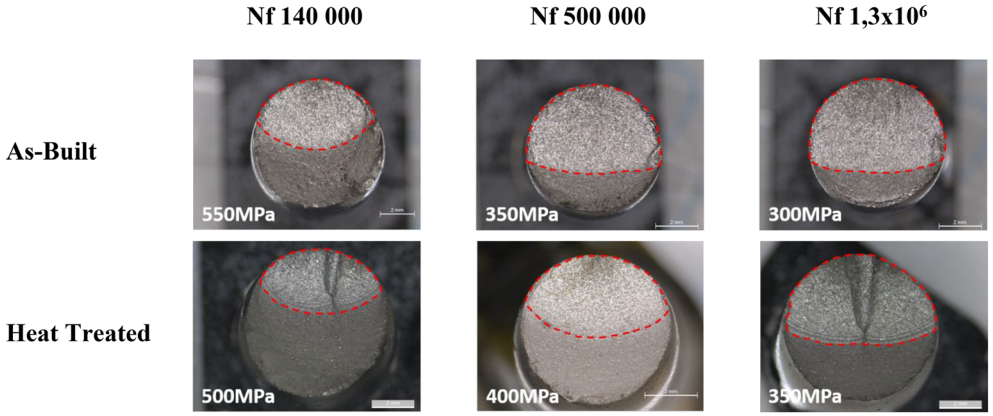

FIGURE 10 Optical images of three as-built and three annealed samples that failed at similar number of cycles. Room temperature high-cycle fatigue tests, $R = 0.1$ [Colour figure can be viewed at wileyonlinelibrary.com]

was 58 μm with a standard deviation of 18 μm for the as-built microstructure and 55 μm with a standard deviation of 22 μm for the annealed microstructure. These sizes are significantly bigger than the voids detected by tomography (13 μm with a standard deviation of 16 μm). The mechanical polishing of the samples is suspected not to have removed the entire as-built LPBF surface, rich in LoFs. Those LoFs hence become critical weakness points.

The resistance of the microstructure to the crack initiation from defects can be quantified by Kitagawa–Takahashi diagrams in literature.[48] For such representation, the size of the initiating defect is quantified by the Murakami's size variable: $\sqrt{Defect\ Area}$.[49] It was shown that there is a minimum defect size for each load level below which the defect is not likely to be the initiation site. Murakami[49] defined this criteria as

$$\sigma_{\text{endurance}} = \frac{1.43 * (\text{Vickers Hardness} + 120)}{\sqrt{Defect\ Area}^{1/6}}.$$

For each sample tested, the defects from which a crack propagated was measured, and their Murakami's size variable were plotted against the load level. The results are given on Figure 12. On the same graph, Murakami's defect size criteria are traced using the Vickers hardness measures of 290 HV for the as-built material and 220 HV on the heat-treated LPBF Inconel 625. It is worth emphasizing that the initiation phase, and thus, the impact of the defects, is known to have a greater influence for long fatigue lives. A particular attention is given to the samples with an endurance greater than 10^6 cycles (<300 MPa for the as built and <375 for the heat treated). At these load levels, the smallest defect to initiate a crack in the as-built samples has a size variable of 50 √μm against 90 √μm for the heat treated. For the heat-treated samples, a defect with a size variable of 50 √μm will initiate a crack only for a load of 500 MPa or higher. Moreover, the as-built samples solicited at 250 MPa have failed with defects of size 102 √μm, which is smaller than the prediction by Murakami criteria. After the heat treatment, no evidence that the samples do not follow the criteria is observed. They even seem to have a better fatigue resistance than the as built, requiring higher load level to initiate on similar sized defects. The heat treatment has hence a beneficial impact on the fatigue life and particularly on the critical defect size for crack initiation. The Murakami criteria predicted the fatigue resistance to decrease with the softening induced by the heat treatment, but the gain in ductility seems to have a greater impact and increases the resistance.

In addition to hardness, as suggested by Murakami, the grain size is a known influencing factor for fatigue life. The as-built LPBF Inconel 625 has an average grain equivalent diameter of 11 μm; the defect is four to five times bigger. For the annealed samples, the defects have an average equivalent diameter of 53 μm, which is closer to the grain size. A small grain size is known to be beneficial to the fatigue life through the Hall–Petch effect notably.[26,32] However, in the case of materials containing cracks or defects, studies show that it is not always the case. In fact, the initiation stage represents between 60% and 90% of the fatigue life in nickel-based alloys.[35] But if the material contains defects of significant size relatively to the microstructure, the crack propagation mechanisms become preponderant.[34,35] The normalized crack length is the number of grains intersected by the crack front. When exceeding 10, the propagation rate increases significantly. In the case of already existing defects among small grains, the crack exceeds this critical value faster than among bigger grains. Moreover, in the case of vertically built LPBF samples, the grains are elongated vertically. The section opposing the crack growth is smaller than the calculated equivalent grain diameter. Hence, the difference in the ratio grains size/defect size can partially explain the difference in fatigue life between the as-built and the annealed microstructures.

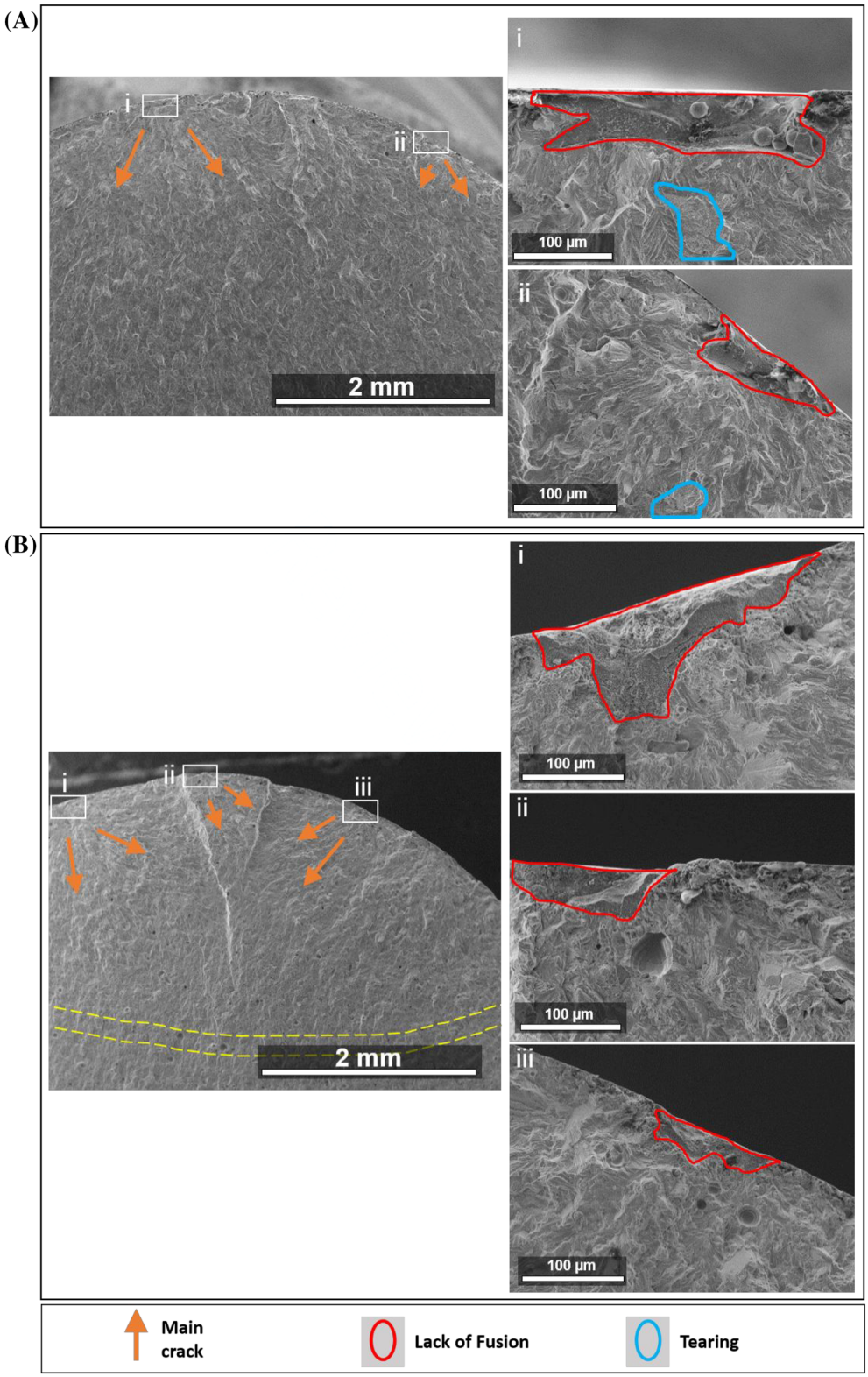

FIGURE 11 Fractographic SEM images of (A) as-built and (B) annealed samples solicited between 45 and 450 MPa. Room temperature high-cycle fatigue tests, $R = 0.1$ [Colour figure can be viewed at wileyonlinelibrary.com]

In terms of crack propagation, the mechanisms in as-built and annealed materials are mainly intragranular cleavage and ridges. Following the surface or subsurface initiation, the propagation veins indicated by the orange arrows on Figure 11 are principally marked by cleavages planes at the crystal scale along with river lines giving the surface a shiny aspect. However, in the as-built samples, punctual zones of tearing with dimple-like texture are spotted in the propagation zones (blue areas on Figure 11A.i and ii). Similar propagation mechanisms were observed in literature for LPBF material.[33] Rather than ductile fracture microvoid coalescence, these zones

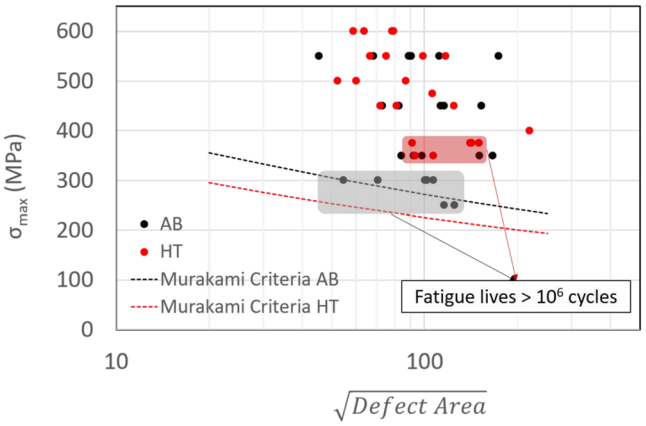

FIGURE 12 Kitagawa–Takahashi diagram representing the size of the defects that initiated a crack against the load level applied on the observed samples: as built (AB) or heat treated (HT). Murakami's criteria for each state are plotted as a dotted line. The size of the defect is represented using the Murakami's defect size variable $\sqrt{Defect\ Area}$ [Colour figure can be viewed at wileyonlinelibrary.com]

are believed to be the tearing of the cellular dendritic structures present in the as-built LPBF Inconel 625 (Figure 2A.ii). As-built LPBF Inconel 625 is heterogeneous, with interdendritic areas enriched in heavy elements, and with a high localized dislocation density. It was shown on cast IN713 that this heterogeneity influences the crack propagation with the contrast of hard interdendritic zones and soft dendritic cores.[32] The interdendritic areas are subject to a localized strengthening, leading to the sudden tearing at the dendritic boundaries. After the annealing treatment, the dendritic structure is dissolved. The material becomes a homogeneous solid solution, hence with a single propagation mechanism.

As introduced in literature,[26,32] the fatigue design of LPBF must take into account the defects, in particular the LoF. Those defects are the initiation sites independently of the heat treatment. The difference in fatigue life between the as-built and the annealed LPBF Inconel 625 cannot be explained on the crack initiation stage. However, the difference in microstructure can explain the difference in behavior. The as built is inhomogeneous, with high density of dislocations entangled around dendritic structures organized in elongated small grains. The annealed LPBF Inconel 625 is homogeneous with twinned grains. The number of grains crossed by the crack front at a given moment is thus higher in the as built, leading to earlier fast long-crack propagation mechanisms.[26,35] Moreover, the crack propagation mechanisms differ, from pure intragranular in the annealed microstructure, to mixed mechanisms with tearing at the interdendritic zones in the as-built microstructure.[29,33]

4.3 | In-service temperature low-cycle fatigue strength

The Morrow diagram given on Figure 7 is plotted from the half-life cycle. For an identical imposed total strain, the as-built LPBF Inconel 625 seems to have a fatigue life similar to the annealed. The logarithmic scale attenuates the difference, and the as-built material has a slightly higher life, especially at low strains.

The cyclic strain–stress response as given on Figure 8 proves a significant difference in the behavior between as-built and annealed microstructures. For low imposed total strains, the as-built LPBF Inconel 625 behaves elastically from the first cycles throughout the test (Figure 8A). The annealed material is subject to plasticity during the first cycles, but the extent of plastic deformation decreases until the response is elastic (Figure 8B). For higher strains, the hysteresis of the annealed material attenuates but does not reach fully elastic response, while the as built has a stable hysteresis shape (Figure 8C,D). Heat-treated Inconel 625 increases its elastic limits through hardening, while as-built Inconel 625 does not show a significant evolution.

In fact, the proportion of plastic deformation is smaller in the as-built response than in the annealed material. The evolution the inelastic strain for the cases of ±0.4% solicitations of as-built and annealed microstructures is given on Figure 13. The as-built material deforms less than 0.08% in the plastic domain throughout the test. For the annealed material, the first cycles have half plastic and half elastic deformation, while the last cycles take up only 0.1% plastic deformation. The proportion of elastic deformation increases significantly.

The tensile properties can explain this difference in behavior for the first cycles. As-built and annealed LPBF Inconel 625 share a similar stiffness but with an initial YTS reaching 510 MPa for the as built and 321 MPa for the annealed. Hence, the as-built material takes up a higher proportion of elastic deformation than plastic deformation to reach the total strain. Moreover, annealed LPBF Inconel 625 is subject to significant hardening, and its YTS increases during the tests. The proportion of plastic deformation decreases, as shown on Figure 13, but not enough to reach the level of as-built material.

The global hardening phenomenon for all strain solicitations level is described on Figure 9. The annealing treatment is necessary to obtain the expected behavior of the superalloy. A work hardening at first, until an inflexion point followed by a second hardening rate up to failure, commonly explained by the precipitation of the γ″ phase.[50] The as-built material is subject to a global hardening too but to a lesser extent. It can be explained by the initial high dislocation density, preventing the work

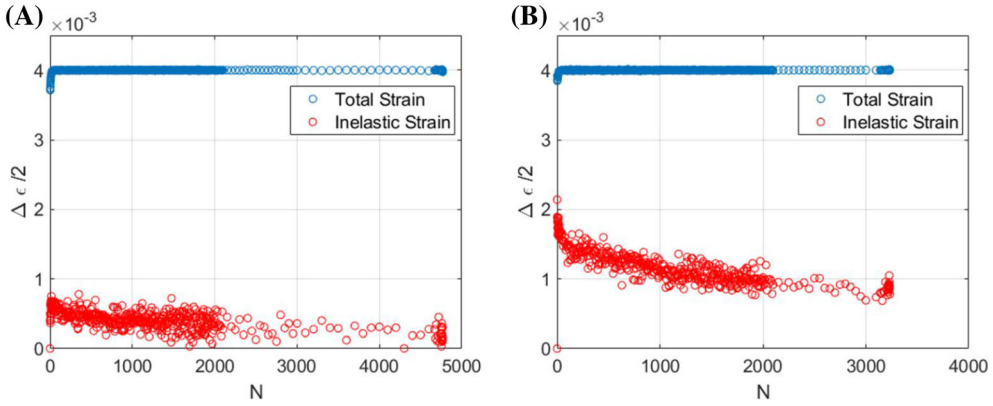

FIGURE 13 Evolution of the total strain and inelastic strain throughout the oligo-cyclic fatigue tests of ±0.4% at 650°C for (A) as-built and (B) annealed LPBF Inconel 625 [Colour figure can be viewed at wileyonlinelibrary.com]

hardening stage. The lack of chemical homogeneity can also modify the kinetic of precipitations[51,52] or the precipitation domains due to the local modification of the chemical composition.[8] Hence, the second stage of hardening is attenuated too.

For a given total strain, as-built and annealed LPBF Inconel 625 do not have the same proportion of elastic and plastic deformation. In order to evaluate the microstructure accommodation, it is more appropriate to consider the inelastic strain instead of the total strain level. For similar inelastic strain, the annealed microstructure shows a better fatigue strength. The Manson–Coffin approximation is translated to the right on Figure 7. The obtained fatigue behavior is similar to conventional Inconel 625.[50]

The fractographic observations have shown that the initiation took place on the surface or subsurface of all service temperature samples, as built or treated. As illustrated by Figure 14, specific defects such as LoFs or carbides were not observed at the initiation sites. The crack initiates on the microstructure. This can be caused by surface residual stresses or testing environment (oxidation) that become an important factor relative to fatigue in the case of low surface roughness.[53]

In fact, service temperature samples were machined from LPBF Inconel 625 ø20-mm bars. The surface defects induced by LPBF, and observed in ambient temperature samples are hence machined off. However, turning of hard alloys induces tensile residual stress in the extreme surface as shown on hard steels,[54,55] Inconel 718,[54,56,57] and more appropriately on AM Inconel 718.[58]

The tensile stressed zone is often balanced by a compressive stress zone on the subsurface.[53,56,58] The level of stress depends on machining parameters[54] or tool wear[56] and can be null under certain optimized conditions.[55,58] The depth affected by tensile residual stresses is thin, well below 100 µm, and is removed by the mechanical polishing applied on the samples. However, polishing can induce new residual surface stresses as well. Few studies of the residual stresses induced by polishing are found in literature, but it was established that they are usually compressive[59,60] and the level increases with the contact force.[60] The polishing set up developed in the laboratory *Institut Clément Ader* and used in this study is made of a rotative felt drill gently put in contact with the turning sample, without applying contact force. The implied compressive stress is hence believed to be minimal, and its influence on the fatigue behavior of the samples is limited. In addition, the temperature of the fatigue tests (650°C) would relieve the slight residual stress.

There were as much multicrack failures as single propagation plane failures, and no correlation to the microstructure state or the load could be drawn. The oxidation color of the open crack depends on the time of exposure and cooling conditions (furnace manually opened or not).

As per at room temperature, the principal propagation mechanism observed were cleavage-like planes or facets and river lines indicating the main crack direction. These mechanisms are identified in literature for LPBF[6] Inconel 625 and other nickel-based superalloys.[35] At a lower scale, striations are visible. In the case of as-built LPBF Inconel, some studies identified them as fatigue striations, due to the propagation of the crack cycle by cycle.[26] Others[33] highlight that striation-like features can be visible on LPBF fracture surface and mistaken for fatigue failure mode, but they correspond to the dendritic microstructure. The crack grows in the interdendritic regions already rich in dislocations, and the failure mode is tearing, not local plasticity and fatigue crack propagation. The results obtained in this study support this claim. In both as-built and treated Inconel 625, fatigue striations are recognizable by their smooth lines and regular step shape and are indicated by the red arrows on Figure 14A.iii,B.ii and iii. However, in the as-built material, other striation-like features were observed. Indicated in yellow on Figure 14A.iii, their direction does not necessarily correspond to the main crack direction, and they are wider

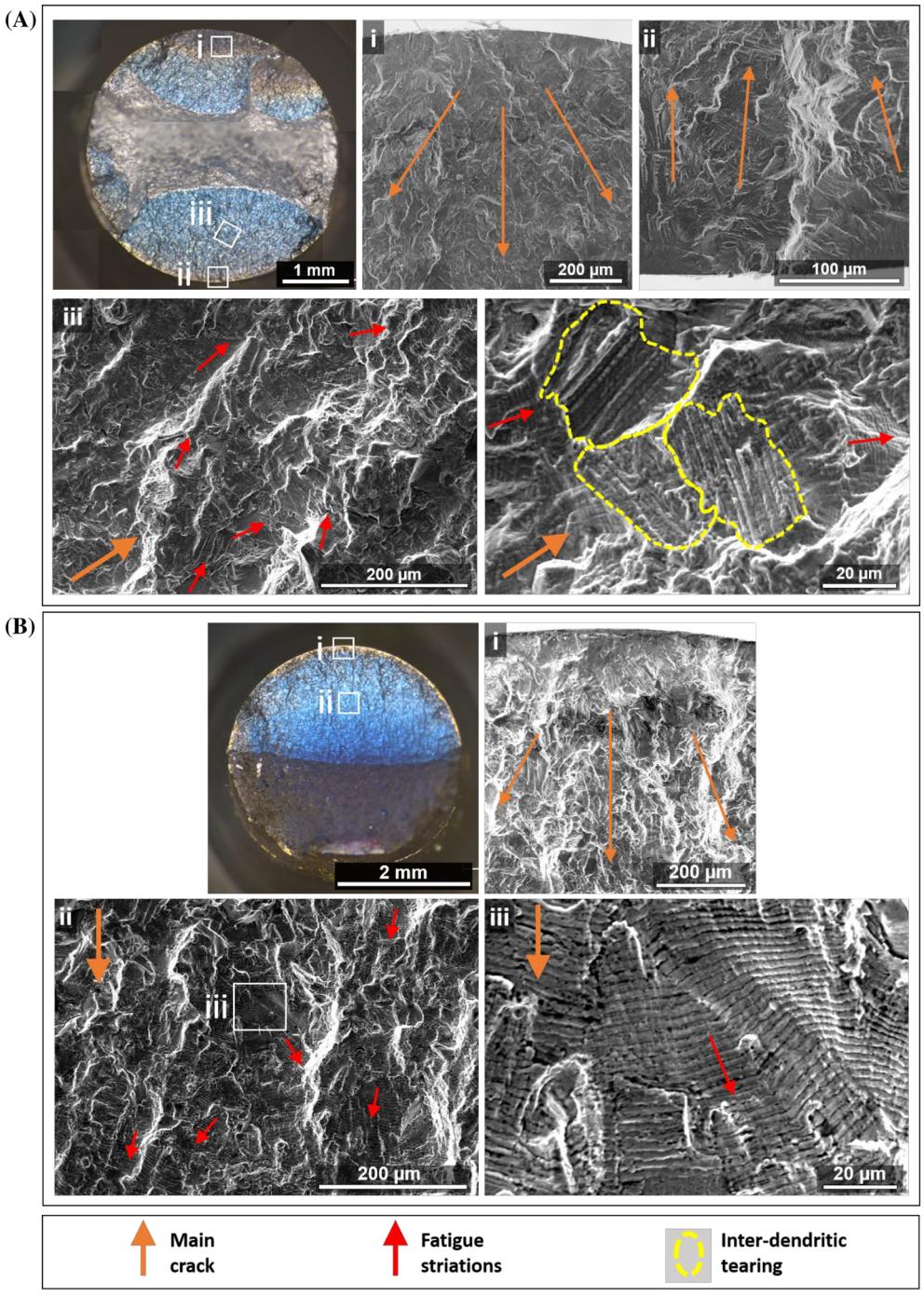

FIGURE 14 Fractographic OM and SEM images: (A) as built, ±0.5% and (B) annealed ±0.4%. $R = -1$, 650°C low-cycle fatigue tests [Colour figure can be viewed at wileyonlinelibrary.com]

than the striations. Their width, of approximately 1 to 2 µm, and organization in zones corresponding to the typical grain size identify them as dendritic microstructure. This type of mechanism is not observed in the treated samples, which display only fatigue striations and river line, typical of fatigue crack propagation in a plastic material. This difference is consistent with the fatigue life and behavior observed, with an annealing treatment that improves ductility and accommodation capacity of the LPBF Inconel 625.

5 | CONCLUSIONS

As-built LPBF Inconel 625 fine and inhomogeneous microstructure leads to high mechanical strength but lower ductility than the conventional alloy. After the annealing heat treatment, the microstructure is homogeneous with twins and equiaxed grains, similar to conventional Inconel 625. This paper presents the experimental investigation of the monotonic tensile properties and fatigue strength at room and in-service (650°C)

temperatures of as-built and annealed microstructures of the LPBF Inconel 625. The impact of the annealing heat treatment on the microstructure and mechanical behavior of LPBF Inconel 625 is fully documented and analyzed, leading to further understanding of the monotonic behavior of the material. Furthermore, the competition between the microstructure and the defects induced by the LPBF process and the consequences on fatigue resistance is investigated with fatigue behavior monitoring and fractographic observations. It led to five major conclusions:

- The PLC effect occurs in LPBF Inconel 625. At room temperature, both as-built and annealed materials have the same behavior. DSA caused by carbon was concluded to be the origin. At high temperatures, as-built material has a critical strain before which the plastic flow is stable. The DSA by molybdenum is identified as the reason. The annealing treatment homogenizes the material, thus removes the critical strain.
- The room temperature high-cycle fatigue strength for the as-built microstructure is lower than 50% of its YTS. After the heat treatment, it reaches 100% of the YTS, close to a theoretical defect free material. The initiation mechanisms are identical in both microstructures, driven by first-order defects that are mostly LoFs open to the surface or in the subsurface. The defects are more noxious in the case of as-built microstructure because of its lack of ductility and the grains being significantly smaller than the defects. Fractography analysis highlighted a better propagation resistance of the crack in annealed material at similar load levels. The as-built material has mix tearing/intragranular propagation mechanisms against pure intragranular in annealed Inconel 625.
- At 650°C, the annealed Inconel 625 microstructure has better low-cycle fatigue strength than as-built microstructure for similar plastic strain. The initiation takes place on the microstructure at the surface of the sample, not on defects.
- As-built LPBF Inconel 625 displays two failure mechanisms: ductile crack propagation with fatigue striations and interdendritic tearing. The annealing treatment prevents the tearing, which is consistent with its better accommodation to plastic strain.
- The fall in mechanical properties of annealed LPBF Inconel 625 complicates the comparison of the fatigue properties for a same total strain. A proposition to use the level of plastic strain as a comparison basis permits to monitor the capacity of the microstructure to accommodate. The annealed microstructure has a better fatigue resistance in this regard.

The difference of fatigue behavior between as-built and annealed LPBF Inconel 625 is mainly attributed to the resistance to crack initiation and propagation. The treated microstructure is subject to hardening and increases its elastic resistance. It permits a better accommodation to the defects and crack tip and increases the propagation resistance. The initiation sites and mechanisms are identical between as-built and annealed material at room and in-service temperatures. The annealing treatment already known to homogenize the tensile monotonic behavior has also a beneficial impact on the fatigue resistance of LPBF Inconel 625.

ACKNOWLEDGMENT

This work was financed and supported by Segula Technologies.

AUTHOR CONTRIBUTIONS

Noémie Martin: conceptualized the study, designed the methodology, validated the data, conducted the formal analysis, conducted the investigation, wrote the original draft of the manuscript, and visualized the study. **Anis Hor**: review and edited the manuscript, designed the methodology, visualized the study, and supervised the study. **Etienne Copin**: review and edited the manuscript. **Philippe Lours**: review and edited the manuscript and supervised the study. **Léon Ratsifandrihana**: review and edited the manuscript and acquired the funding.

DATA AVAILABILITY STATEMENT

The data that support the findings of this study are available from the corresponding author upon reasonable request.

NOMENCLATURE

AM	additively manufactured
DSA	dynamic strain aging
EBSD	electron backscattered diffraction
EDX	energy-dispersive X-ray analysis
IPF	inverse pole figure
KAM	kernel average misorientation
LoF	lack of fusion
LPBF	laser-based powder bed fusion
PLC	Portevin–Le Châtelier effect
SEM	scanning electron microscopy
TEM	transmission electron microscopy

REFERENCES

1. Davis JR (Ed). *ASM Specialty Handbook: Nickel, Cobalt, and Their Alloys*. Vol. 38. ASM International Handbook Committee; 2013.
2. Belan J. GCP and TCP phases presented in nickel-base superalloys. *Mater Today Proc*. 2016;3(4):936-941.
3. Sateesh NH, Kumar GM, Prasad K, Srinivasa CK, Vinod AR. Microstructure and mechanical characterization of laser sintered Inconel-625 superalloy. *Procedia Mater Sci*. 2014;5: 772-779.
4. Gonzalez JA, Mireles J, Stafford SW, Perez MA, Terrazas CA, Wicker RB. Characterization of Inconel 625 fabricated using powder-bed-based additive manufacturing technologies. *J Mater Process Technol*. 2019;264:200-210.
5. Witkin DB, Patel D, Albright TV, Bean GE, McLouth T. Influence of surface conditions and specimen orientation on high cycle fatigue properties of Inconel 718 prepared by laser powder bed fusion. *Int J Fatigue*. 2020;132:105392.
6. Poulin J, Brailovski V, Terriault P. Long fatigue crack propagation behavior of Inconel 625 processed by laser powder bed fusion: influence of build orientation and post-processing conditions. *Int J Fatigue*. 2018;116:634-647.
7. Marchese G, Parizia S, Rashidi M, et al. The role of texturing and microstructure evolution on the tensile behavior of heat-treated Inconel 625 produced via laser powder bed fusion. *Mater Sci Eng A*. 2020;769:138500.
8. Marchese G, Lorusso M, Parizia S, et al. Influence of heat treatments on microstructure evolution and mechanical properties of Inconel 625 processed by laser powder bed fusion. *Mater Sci Eng A*. 2018;729:64-75.
9. Lee J, Terner M, Jun S, Hong H-U, Copin E, Lours P. Heat treatments design for superior high-temperature tensile properties of alloy 625 produced by Selective Laser Melting. *Mater Sci Eng A*. 2020;790:139720.
10. Pleass C, Jothi S. Influence of powder characteristics and additive manufacturing process parameters on the microstructure and mechanical behaviour of Inconel 625 fabricated by Selective Laser Melting. *Addit Manuf*. 2018;24:419-431.
11. Nakada Y, Keh AS. Serrated flow in Ni-C alloys. *Acta Metall*. 1970;18(4):437-443.
12. Cui C, Zhang R, Zhou Y, Sun X. Portevin-Le Châtelier effect in wrought Ni-based superalloys: experiments and mechanisms. *J Mater Sci Technol*. 2020;51:16-31.
13. Rai RK, Sahu JK. Mechanism of serrated flow in a cast nickel base superalloy. *Mater Lett*. 2018;210:298-300.
14. Zhao R, Han JQ, Liu BB, Wan M. Interaction of forming temperature and grain size effect in micro/meso-scale plastic deformation of nickel-base superalloy. *Mater Des*. 2016;94: 195-206.
15. Zhao S, Li X, Rong L. Serrated flow induced by twin boundary-slip band interactions in a FeNi-base austenitic alloy. *Mater Lett*. 2011;65(15–16):2388-2390.
16. Beese AM, Wang Z, Stoica AD, Ma D. Absence of dynamic strain aging in an additively manufactured nickel-base superalloy. *Nat Commun*. 2018;9(1):1-8.
17. Kim KS, Kang TH, Kassner ME, Son KT, Lee KA. High-temperature tensile and high cycle fatigue properties of Inconel 625 alloy manufactured by laser powder bed fusion. *Addit Manuf*. 2020;35:101377.
18. Stromeyer CE. The determination of fatigue limits under alternating stress conditions. *Proc R Soc A*. 1914;90:411-425.
19. Li HF, Yang SP, Zhang P, Liu YQ, Wang B, Zhang ZF. Material-independent stress ratio effect on the fatigue crack growth behavior. *Eng Fract Mech* 2022; 259, 108116. 10.1016/j. engfracmech.2021.108116.
20. Shrestha R, Simsiriwong J, Shamsaei N. Fatigue behavior of additive manufactured 316L stainless steel under axial versus rotating-bending loading: synergistic effects of stress gradient, surface roughness, and volumetric defects. *Int J Fatigue*. 2021; 144:106063.
21. Andras A Comparison of low cycle axial, rotating and bending fatigue of aluminium alloys. *Low Cycle Fatigue and Elasto-Plastic Behaviour of Materials*. 1987. Springer. doi: 10.1007/978-94-009-3459-7_94
22. Bathias C. There is no infinite fatigue life in metallic materials. *Fatigue Fract Eng Mater Struct*. 1999;22(7):559-565.
23. Theriault A, Xue L, Dryden JR. Fatigue behavior of laser consolidated IN-625 at room and elevated temperatures. *Mater Sci Eng A*. 2009;516(1-2):217-225.
24. Koutiri I, Pessard E, Peyre P, Amlou O, De Terris T. Influence of SLM process parameters on the surface finish, porosity rate and fatigue behavior of as-built Inconel 625 parts. *J Mater Process Tech*. 2018;255:536-546.
25. Pereira Lima FG, Lourenço JM, Maribondo do Nascimento R, Castro NA. Fracture behavior and fatigue performance of inconel 625. *Mater Res*. 2018;21(4). https://doi.org/10.1590/1980-5373-mr-2017-1089
26. Poulin JR, Kreitcberg A, Terriault P, Brailovski V. Fatigue strength prediction of laser powder bed fusion processed Inconel 625 specimens with intentionally-seeded porosity: feasibility study. *Int J Fatigue*. 2020;132:105394.
27. Jiménez M, Ludwig W, Gonzalez D, Molina-Aldareguia JM. The role of slip transfer at grain boundaries in the propagation of microstructurally short fatigue cracks in Ni-based superalloys. *Scr Mater*. 2019;162:261-265.
28. Trester P, Kaae J, Gallix R. Fatigue strength of Inconel 625 plate and weldments used in the DIII-D configuration vacuum vessel. *J Nucl Mater*. 1985;134:347-350.
29. Yadollahi A, Shamsaei N. Additive manufacturing of fatigue resistant materials: challenges and opportunities. *Int J Fatigue*. 2017;98:14-31.
30. Genée J, Signor L, Villechaise P. Slip transfer across grain/twin boundaries in polycrystalline Ni-based superalloys. *Mater Sci Eng A* 2017;701: 24-33. doi:10.1016/j.msea.2017.06.072
31. Nadot Y, Nadot-Martin C, Dragon A, Vincent M. Competition between surface defect and grain size under fatigue loading-ARMCO iron. *Procedia Struct Integr*. 2017;7:530-535.
32. Liu G, Winwood S, Rhodes K, Birosca S. The effects of grain size, dendritic structure and crystallographic orientation on fatigue crack propagation in IN713C nickel-based superalloy. *Int J Plast*. 2020;125:150-168.
33. Calmunger M, Eriksson R, Lindstr T, Leidermark D. Effect of additive manufacturing on fatigue crack propagation of a gas turbine superalloy. *Procedia Struct Integrity*. 2019;23: 215-220.
34. Rackwitz J, Yu Q, Yang Y, et al. Effects of cryogenic temperature and grain size on fatigue-crack propagation in the medium-entropy CrCoNi alloy. *Acta Mater*. 2020;200:351-365.

35. Zhu X, Gong C, Jia YF, et al. Influence of grain size on the small fatigue crack initiation and propagation behaviors of a nickel-based superalloy at 650°C. *J Mater Sci Technol*. 2019; 35(8):1607-1617.
36. Sánchez Camargo MC. Mechanical multi-scale characterization of metallic materials by nanoindentation test. 2019.
37. Fang XY, Li HQ, Wang M, Li C, Guo YB. Characterization of texture and grain boundary character distributions of selective laser melted Inconel 625 alloy. *Mater Charact*. 2018;143: 182-190.
38. Nguejio J, Szmytka F, Hallais S, Tanguy A, Nardone S, Godino MM. Comparison of microstructure features and mechanical properties for additive manufactured and wrought nickel alloys 625. *Mater Sci Eng A*. 2019;764:138214.
39. Li C, White R, Fang XY, Weaver M, Guo YB. Microstructure evolution characteristics of Inconel 625 alloy from selective laser melting to heat treatment. *Mater Sci Eng A*. 2017;705: 20-31.
40. Voisin T, Forien JB, Perron A, et al. New insights on cellular structures strengthening mechanisms and thermal stability of an austenitic stainless steel fabricated by laser powder-bed-fusion. *Acta Mater*. 2021;203:116476.
41. Godec M, Malej S, Feizpour D, et al. Hybrid additive manufacturing of Inconel 718 for future space applications. *Mater Charact*. 2021;172:110842.
42. Max B Comportement mécanique et couplage mécanique-oxydation dans l'alliage 718: effet des éléments en solution solide. 2014: 206.
43. Murakami Y, Takagi T, Wada K, Matsunaga H. Essential structure of S-N curve: prediction of fatigue life and fatigue limit of defective materials and nature of scatter. *Int J Fatigue*. 2021; 146:106138.
44. Strzelecki P. Determination of fatigue life for low probability of failure for different stress levels using 3-parameter Weibull distribution. *Int J Fatigue*. 2021;145:106080.
45. Van Den Beukel A, Kocks UF. The strain dependence of static and dynamic strain-aging. *Acta Metall*. 1982;30(5):1027-1034.
46. Kim IS, Chaturvedi MC. Serrated flow in Inconel 625. *Trans Japan Inst Met*. 1987;28(3):205-212.
47. Shankar V, Valsan M, Rao KBS, Mannan SL. Effects of temperature and strain rate on tensile properties and activation energy for dynamic strain aging in alloy 625. *Metall Mater Trans A Phys Metall Mater Sci* 2004;35(10):3129-3139.
48. Pessard E, Gerin B, Morel F, Verdu C. *Effets des défauts géométriques et des gradients de microstructure et de contraintes sur le comportement en fatigue de composants forgés et grenaillés Colloque MECAMAT 2017*. MECAMAT; 2017.
49. Murakami Y. Chapter 4—effect of size and geometry of small defects on the fatigue limit. In: Murakami Y, ed. *Metal Fatigue*. Elsevier Science Ltd; 2002:35-55.
50. Mataveli L, Cormier J, Bertheau D, et al. High temperature low cycle fatigue properties of alloy 625. *Mater Sci Eng A*. 2016;650: 161-170.
51. Yenusha CO, Ji Y, Liu Y, et al. Three-dimensional phase-field simulation of γ'' precipitation kinetics in Inconel 625 during heat treatment. *Comput Mater Sci*. 2021;187:110123.
52. Lindwall G, Campbell CE, Lass EA, et al. Simulation of TTT curves for additively manufactured Inconel 625. *Metall Mater Trans A Phys Metall Mater Sci*. 2019;50(1):457-467.
53. Novovic D, Dewes RC, Aspinwall DK, Voice W, Bowen P. The effect of machined topography and integrity on fatigue life. *Int J Mach Tool Manuf*. 2004;44(2–3):125-134.
54. Outeiro JC, Pina JC, M'Saoubi R, Pusavec F, Jawahir IS. Analysis of residual stresses induced by dry turning of difficult-to-machine materials. *CIRP Ann - Manuf Technol*. 2008;57(1): 77-80.
55. Valiorgue F, Zmelty V, Dumas M, et al. Influence of residual stress profile and surface microstructure on fatigue life of a 15-5PH. *Procedia Eng*. 2018;213:623-629.
56. Madariaga A, Kortabarria A, Hormaetxe E, Garay A, Arrazola PJ. Influence of tool wear on residual stresses when turning Inconel 718. *Procedia CIRP*. 2016;45:267-270.
57. Careri F, Imbrogno S, Umbrello D, Outeiro JC, Batista AC. A residual stress prediction of machining IN718 produced by direct energy deposition. *Procedia CIRP*. 2021;102:13-18.
58. Careri F, Imbrogno S, Umbrello D, Attallah MM, Outeiro J, Batista AC. Machining and heat treatment as post-processing strategies for Ni-superalloys structures fabricated using direct energy deposition. *J Manuf Process*. 2021;61:236-244.
59. Minguela J, Slawik S, Mücklich F, et al. Evolution of microstructure and residual stresses in gradually ground/polished 3Y-TZP. *J Eur Ceram Soc*. 2020;40(4):1582-1591.
60. Huang Y, Xiao G, Zhao H, et al. Residual stress of belt polishing for the micro-stiffener surface on the titanium alloys. *Procedia CIRP*. 2018;71:11-15.